Asian Journal of Water, Environment and Pollution. Vol. 22, No. 4 (2025), pp. 28-40.
doi: 10.36922/AJWEP025190147

ORIGINAL RESEARCH ARTICLE

Spatiotemporal variability and climate forcing mechanisms of wind and solar energy in northwest China

Shuyue Qin[1†], Bingyue Wen[1†*], Wei Bao[1], Xuexian Wang[1], Zihan Yang[2], Ruei-Yuan Wang[3], Hongbei Guo[4], Dongping Yu[1], Yanfang Jin[1], Yunxia Ma[5], and Taohui Li[2*]

[1]Unit of Sino-British Cooperative, School of International Business, Yunnan University of Finance and Economics, Kunming, Yunnan, China
[2]Yunnan Key Laboratory of Meteorological Disasters and Climate Resources in the Greater Mekong Subregion, School of Earth Science, Yunnan University, Kunming, Yunnan, China
[3]Department of Geography, School of Science, Guangdong University of Petrochemical Technology, Maoming, Guangdong, China
[4]Department of Marxism, School of Marxism, Southwest Forestry University, Kunming, Yunnan, China
[5]Yunnan Key Laboratory of Plateau Geographic Processes and Environmental Change, Faculty of Geography, Yunnan Normal University, Kunming, Yunnan, China
***Corresponding authors:** Bingyue Wen (wenbingyue@ynufe.edu.cn)
Taohui Li (taohui0813@foxmail.com)
[†]These authors contributed equally to this work.

Received: May 8, 2025; Revised: May 30, 2025; Accepted: June 5, 2025; Published online: July 2, 2025

Abstract: As a pivotal region for China's wind and solar energy strategic deployment, northwest China holds critical importance in the national energy transition. Our integrated analysis reveals concerning multidecadal declines in wind energy resources (WER) and solar energy resources (SER) – climate-sensitive parameters requiring urgent mechanistic elucidation. Through the synergistic application of meteorological station networks, reanalysis datasets, and machine learning architectures, we establish three key findings: (i) both resources demonstrate regime shifts with distinct phases – initial growth, transitional decline, and accelerated depletion – superimposed with significant 29 – 30-year oscillation signals (wavelet analysis); (ii) WER and SER display marked differences in spatial evolution; WER shows an increasing trend from south to north, while SER shows a decreasing trend from the central region to the surrounding areas; and (iii) the main controlling factors of WER have shifted from air–sea cycle dominance to inter-regional climate variability, while SER exhibits the opposite trend. This is mainly attributed to a significant reduction in cloud cover and a marked decrease in the rate of increase of the daily maximum temperature. This study demonstrates that synoptic-scale circulation reorganizations override local anthropogenic impacts in determining the viability of renewable energy resources.

Keywords: Global warming; Wind energy resources; Solar energy resources; Spatiotemporal characteristics; Driving mechanism

1. Introduction

Against the backdrop of intensifying global climate change, China has formally announced its "Dual Carbon Goals" (peaking carbon emissions by 2030 and achieving carbon neutrality by 2060), prioritizing energy structure transformation through accelerated clean energy adoption and phased fossil fuel reduction.[1-4] As two technologically mature and globally scalable renewable energy sources, wind and solar power have undergone rapid deployment in China's energy matrix.[5-7] Notably, these climate-dependent resources exhibit strong spatiotemporal variability influenced by atmospheric dynamics and surface–atmosphere interactions.[8,9]

Meteorological records over the past five decades reveal concerning trends: A persistent decline in terrestrial wind speeds and diminishing annual total solar radiation (TSR) across mainland China, with particularly marked reductions in northwest China (NWC).[8] While urbanization-induced surface modifications (such as increased albedo and aerodynamic roughness) are recognized contributing factors, NWC presents a counterintuitive case study.[10,11] This region has maintained relatively stable urbanization levels since 1987 while experiencing a paradoxical "warm–wet transition" climate shift.[12] This decoupling suggests that synoptic-scale circulation changes may dominate over local anthropogenic impacts in driving renewable energy resource depletion in NWC.[12,13]

Present research paradigms exhibit two critical limitations: (i) overemphasis on continental/global-scale analyses, which obscures regional climate zone specificities, particularly in arid regions with optimal renewable energy resource development potential;[5,6] and (ii) methodological constraints that favor short-term (<10 years) observational datasets over decadal-scale climate pattern analyses,[9,10] while also neglecting differences across climate zones, especially in arid areas where the wind energy resources (WER) and solar energy resources (SER) are abundant and conditions for their development and utilization are more favorable.[14,15] Addressing these knowledge gaps is imperative for developing climate-resilient renewable energy strategies in vulnerable ecotones.

In summary, to explain the significant decline in WER and SER in NWC over the past half century, this study takes NWC as the study area and applies trend analysis, spectral analysis, and random forest (RF) modeling to examine the evolution characteristics of WER and SER in NWC from 1961 to 2019. It further analyzes the climate-driving mechanisms underlying the significant decline in WER and SER from the perspective of climate change. This study aims to answer two key questions: (i) what are the temporal and spatial evolution patterns of WER and SER under the background of a warm and humid climate in NWC? and (ii) What are the climate-driving mechanisms of the WER and SER in NWC changes on an interannual scale in NWC?

2. Materials and methods

2.1. Study area

NWC is an important part of the arid region of Central Asia (73°25'–110°55'E, 31°35'–49°15'N), accounting for about one-third of China's land area (Figure 1). The region is deeply inland, far from the ocean, and surrounded by high mountains, which block the inflow of moist oceanic air. It exhibits a typical continental climate and is thus the driest area in China.[16,17] Although the region is rich in WER and SER, and the climate has shown a trend of warming and humidification in recent decades, both WER and SER in the region have been gradually decreasing.[18,19]

2.2. Data sources

Daily sunshine duration, average wind speed, and average air pressure data were obtained from the China Surface Climate Data Daily Value Dataset V3.0. In this study, data pre-processing was conducted by discarding sites with significant data loss. The exclusion criterion was that sites with more than 20% missing data over the time series were removed. For stations with <20% missing data, linear interpolation was performed using data from adjacent years. The interpolated results were then compared with and corrected using the climatic research unit (CRU) dataset. After this pre-processing, a total of 400 meteorological stations with complete sunshine duration and average wind speed data from 1961 to 2019 were selected.

In addition, to explore the climate-driving mechanisms behind WER and SER in NWC, relevant data on atmospheric circulation (ASC) and climate change were collected based on existing research. The ASC index data were sourced from the National Oceanic and Atmospheric Administration, United States of America (http://www.esrl.noaa.gov/psd/enso/). To supplement climate indicators such as cloud cover, the study also utilized CRU's 100-year sequence grid dataset (http://www.cru.uea.ac.uk/data/). The time series for all the above data spans from 1961 to 2019.

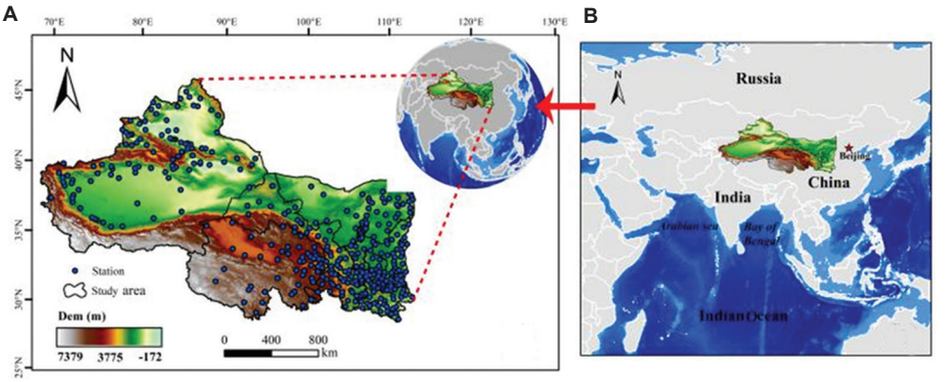

Figure 1. Distribution of meteorological stations (A) and geographical location (B) in the study area
Note: The Arcgis10.8 software was used in this study. The map data were obtained from the China Standard Map Service System. Drawing review No: GS(2020)4619.

2.2.1. Effective wind energy density (EWED)
When the wind speed ranges from 3 to 20 m/s, the kinetic energy of the airflow per unit area and unit time is referred to as the EWED.[10,18] The EWED is calculated using the following formula:

$$W = \frac{1}{2n}\sum_{i=1}^{n}\rho V_i^3 \quad \text{(I)}$$

where W is the EWED (W/m^2), ρ is the air density (kg/m^3), V is the average wind speed (m/s), and n is the total number of days when the average wind speed is within the range of 3 – 20 m/s.

This study used daily average air pressure and daily average temperature data from the dataset to calculate the daily air density ρ at each site. The formula used is as follows:

$$\rho = \frac{P}{R \times T} \quad \text{(II)}$$

In this equation, ρ is the daily air density (kg/m^3), P is the daily average air pressure (Pa or N/m^2), R is the gas constant for air (287 J/[kg·K]), and T is the daily average temperature in Kelvin (°C + 273).

2.2.2. TSR
Based on sunshine duration, this study adopted the methods of Lv *et al.*[8] to calculate the TSR and subsequently computed the annual average TSR using summation and averaging methods.[10,19] The formula is as follows:

$$Q = \sum_{i=1}^{n} R_i S_i \quad \text{(III)}$$

where Q is the total solar annual radiation (MJ·m^{-2}), R is the daily TSR (MJ·m^{-2}), S is the sunshine percentage, and n is the ordinal number of days in a year. The daily TSR R is calculated using:

$$R = I\,E\,(\omega \sin\phi \sin\delta + \cos\phi \sin\omega)/\pi \quad \text{(IV)}$$

where R is the daily TSR (MJ·m^{-2}), E is the average distance between the sun and Earth (1.4966 × 10^8 m), δ is the solar declination, Φ is the geographical latitude, ω is the hour angle at sunset, I is the solar constant, set to 1,367 W/m^2 (118.109 MJ·m^{-2}·d^{-1}), and ϖ is the mathematical constant (3.14159). The sunshine percentage S is calculated as:

$$S = \frac{H}{(2/15)\omega} \quad \text{(V)}$$

where H is the sunshine duration (hours), and ω is the hour angle at sunset.

2.3. Research methods

2.3.1. Analysis of change trend
The Mann–Kendall (MK) non-parametric test was employed to assess long-term trends and detect abrupt shifts in environmental variables. This rank-based methodology, which does not require the assumption of a normal distribution and is robust against outliers, has been extensively validated for hydroclimatic time series analysis.[20,21] Its computational reliability accounts for its widespread application in identifying climate-induced changes and system transitions in meteorological and hydrological research. The formula is as follows:

$$S_k = \sum_{i=1}^{k}\sum_{i=1}^{i-1} a_{ij}\,(k = 2,3,\ldots,n) \quad \text{(VI)}$$

$$a_{ij} = \begin{cases} 1, x_i > x_j \\ 0, x_i \le x_j \end{cases} j = 1,2,3,...,i \quad \text{(VII)}$$

Here, S_k is the cumulative number of times the value at time i exceeds the value at time j. When $k = 1$, $S_1 = 0$. Assuming the time series is randomly independent, the statistical variables are defined as:

$$UF_k = \frac{S_k - E(S_k)}{\sqrt{Var(S_k)}} k = 2,3,...,n \quad \text{(VIII)}$$

where UF_k is the test statistic, with $UF_1 = 0$; $E(S_k)$ and $Var(S_k)$ are the mean and variance of cumulative S_k. For a time series X_1, X_2, orX_n that is independent and identically distributed, $E(S_k)$ and $Var(S_k)$ are calculated as:

$$\begin{cases} E(S_k) = \dfrac{n(n+1)}{4} \\ Var(S_k) = \dfrac{n(n-1)(2n+5)}{72} \end{cases} \quad \text{(IX)}$$

The *UF* statistic is computed in the forward direction of the time series $X_1, X_2, ..., X_n$, while *UB* is computed in reverse order. At a significance level of $\alpha = 0.05$, the critical value is 1.96. If $|UF|>1.96$, a significant trend is indicated. Specifically, if $UF > 0$, the sequence shows an upward trend, $UF < 0$ indicates a downward trend, and $UF = 0$ indicates no trend. If $UF > 1.96$, the sequence shows a significant upward trend; if $UF <-1.96$, it exhibits a significant downward trend. An intersection point between the positive sequence (*UF*) and negative sequence (*UB*) curves within the critical values indicates the mutation start time.

2.3.2. Wavelet analysis

To calculate the real part of the wavelet, this study used the Morlet continuous complex wavelet as the basis function (i.e., the comr function).[12,21] It is expressed as follows:

$$comr(x) = \frac{\sigma^{2i\pi F_e} \times \dfrac{X^2}{F_b}}{\sqrt{\pi F_b}} \quad \text{(X)}$$

$$Var(a) = \int_{-\infty}^{\infty} \omega_f \left|(a,b)\right|^2 db \quad \text{(XI)}$$

where F_e is the center frequency, and F_b is the frequency bandwidth. The wavelet square difference is denoted V_{ar}, and is obtained by integrating the square of the wavelet coefficient over the time translation domain b.

2.3.3. RF modeling

The RF algorithm – an ensemble learning framework initially conceptualized by Breiman – operates through parallelized decision trees to enhance predictive accuracy while enabling robust quantification of feature importance.[20] By implementing a bagging technique, the model iteratively generates bootstrapped training subsets and incorporates stochastic feature selection during tree construction, ultimately aggregating predictions through majority voting to mitigate overfitting risks. For this investigation, multivariate feature importance analysis was performed using the Ranger package within the tidymodels environment, systematically identifying the dominant drivers underlying the spatiotemporal dynamics of WER and SER.

Furthermore, existing studies[22,23] have shown that the decrease in cloud cover, increases in atmospheric water vapor, and interannual variations in monsoon circulation are the main causes of direct changes in SER and WER. Therefore, nine climatic factors were selected for attribution analysis, including temperature, precipitation, cloud fraction, relative humidity, and ASC.

3. Results

3.1. Temporal variation characteristics of WER and SER

In this study, two indicators (EWED and annual TSR) were used, in combination with the Mann–Kendall trend test and spectral analysis methods, to map the temporal evolution of EWED and annual TSR in NWC from 1961 to 2019 (Figures 2 and 3). The trend analysis results (Figure 2A and B, Table 1) showed that both EWED and annual TSR in NWC exhibited a significant decreasing trend over the period 1961 – 2019, with average annual decline rates at 0.598 $W \cdot m^{-2} \cdot a^{-1}$ ($R^2 = 0.718$) and 5.663 $MJ \cdot m^{-2} \cdot a^{-1}$ ($R^2 = 0.429$), respectively. The Mann–Kendall trend test results indicate that the interannual variations in EWED and annual TSR in NWC over the past half-century can be divided into three stages: A slow increase stage (stage I), a slow decrease stage (stage II), and a rapid decrease stage (stage III). The specific results are as follows: For EWED, stage I spanned 1961 – 1984, and for annual TSR, it spanned 1961 – 1975. During this period, the UF values were mostly >0, indicating an increasing trend. Stage II spanned 1985 – 1992

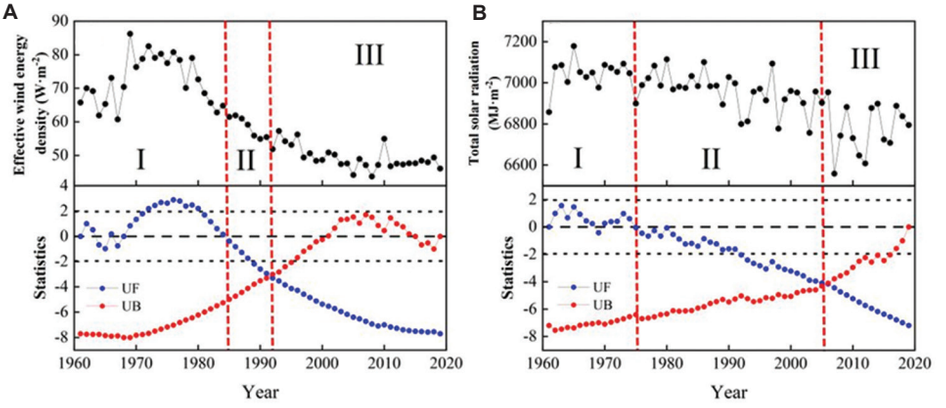

Figure 2. Temporal characteristics of (A) wind and (B) solar energy resources from 1961 to 2019
Note: UF/UB represents the statistical values calculated based on the ascending/descending order of the time series.

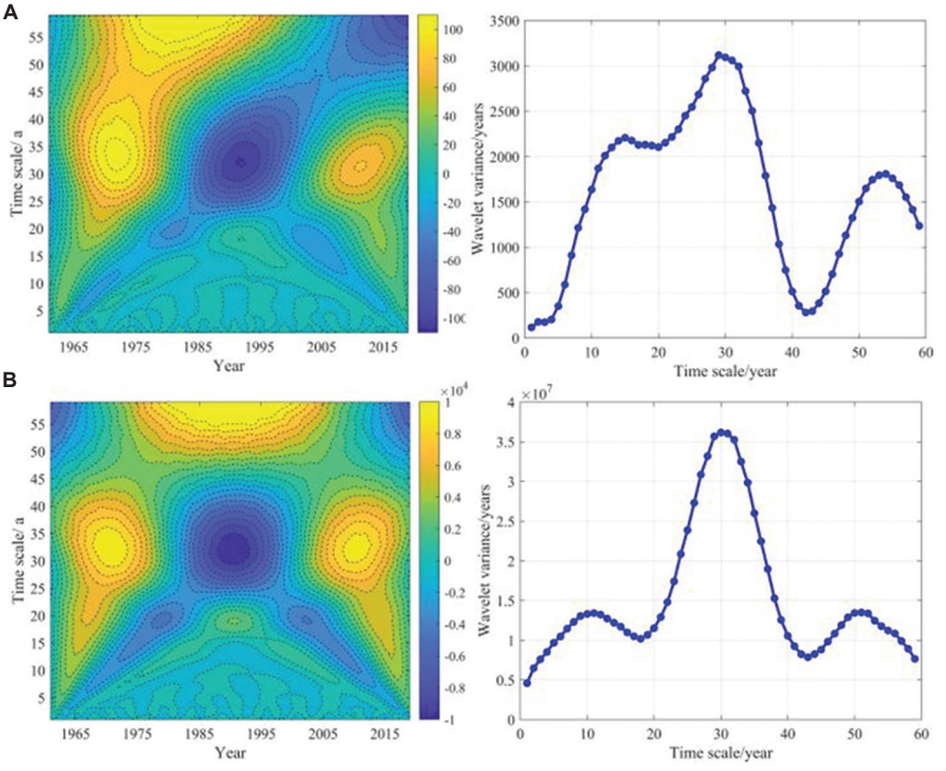

Figure 3. Wavelet analysis of the (A) wind and (B) solar energy resources from 1961 to 2019

Table 1. Feature statistics of wind and solar energy resources in the time series

Index	Central frequency domain scale	Principal period of oscillation	Abrupt change year	UF	Interannual variation	Variation trend
Wind	25 – 40 years	29 years	1991	<−1.96	$-0.598 W \cdot m^{-2} \cdot a^{-1}$	Significant decrease
Solar	23 – 44 years	30 years	2005	<−1.96	$-5.663 MJ \cdot m^{-2} \cdot a^{-1}$	Significant decrease

for EWED and 1975 – 2006 for annual TSR, during which UF values were <0, and a sudden change point was observed, indicating the beginning of a downward trend. Stage III spanned 1992 – 2019 for EWED and 1975 – 2019 for annual TSR, with UF values below −1.96, indicating a significant downward trend.

The periodic analysis results of the EWED and the annual TSR in NWC from 1961 to 2019 (Figure 3A and B, Table 1) showed that, on this timescale, the EWED and annual TSR exhibited significant positive and negative phase alternations during cycles of 25 – 40 years and 23 – 44 years, respectively. Meanwhile, the wavelet variance results indicate that the EWED and the TSR in NWC have significant main oscillation periods of 29 and 30 years, respectively. This suggests that the periodic variation of EWED in NWC is faster than that of TSR. The influence of climate change and other factors on the interdecadal variation of TSR may be limited, whereas the EWED demonstrated a higher periodic frequency.

The table also shows that both WER and SER in NWC are decreasing year by year, with stable periodic changes. Overall, over the past half-century, WER and SER in NWC have exhibited a significant downward trend, accompanied by a pronounced main cycle change, indicating potential future changes in WER and SER in the region. These findings highlight the need for further simulation analyses incorporating additional influencing factors.

3.2. Spatial variation characteristics of wind and SER

In this study, the multi-year average values of EWED and annual TSR in NWC from 1961 to 2019 were calculated. Based on the inverse distance weighting model in ArcGIS 10.8 software, spatial distribution maps of EWED and annual TSR for NWC were generated (Figure 4). The results in Figure 4A and B show that EWED in NWC generally increases from south to north. In most areas, EWED ranged between 0 and 100 $W \cdot m^{-2}$, while in Xinjiang and northern Inner Mongolia, it exceeded 100 $W \cdot m^{-2}$. The region with the smallest decreasing trend in EWED (−0.26 $W \cdot m^{-2} \cdot a^{-1}$) is located in the southern part of the northwest region, including southern Qinghai, Gansu, and Shaanxi provinces. In contrast, Xinjiang and northern Inner Mongolia (regions with high EWED) also exhibited the most significant decreasing trend (−1.44 $W \cdot m^{-2} \cdot a^{-1}$). The results in Figure 4C and D indicate that the spatial distribution patterns of annual TSR and EWED in NWC differed. TSR generally decreases from the central region toward the northwest and southeast. In most areas, annual TSR ranged from 5,650 to 6800 $MJ \cdot m^{-2}$, while in southern Shaanxi, it fell below 5,000 $MJ \cdot m^{-2}$. The region with the most significant decrease in annual TSR (−28.12 $W \cdot m^{-2} \cdot a^{-1}$) was in southwestern Qinghai, whereas the northern part of Gansu province, which has higher TSR levels, showed the smallest decreasing trend (−7.86 $W \cdot m^{-2} \cdot a^{-1}$).

3.3. Climate-driving mechanisms of wind and SER

To understand the climate-driving mechanisms of WER and SER in NWC on an interannual scale, existing climate indicators were selected for correlation analysis. The results (Table 2) showed that, in the 2-time series (before and after the abrupt change), WER and climate factors in NWC exhibited opposite trends. Before the abrupt change, the correlation between the ASC and WER was high. After the change, WER showed relatively strong correlations with cloud cover and relative humidity. In contrast, the correlation between SER and climatic factors exhibited a pattern opposite to that of WER. Before the mutation, SER was more strongly correlated with relative humidity, while after the mutation; SER correlation with the ASC became relatively high. Based on relevant research, these results suggest that the driving influence of climate factors on the WER and SER may vary due to feedback mechanisms at the water–soil–air interface in the region, influenced by global warming, which in turn alters the dominant climatic control factors.

In addition, due to the spatial heterogeneity of topography and altitude in the northwest region, there were significant differences in climate distribution and characteristics. As a result, WER and SER in the northwest region were affected by the interaction of multiple climatic factors. Regression analysis among these factors may lead to multicollinearity issues, thereby reducing the explanatory power of individual climatic factors on the interannual variation of WER and SER. To address this, the RF model, based on the ranger package in R, was used to calculate the importance of various climate factors on WER and SER at the interannual scale. The dominant influencing factors were then identified based on their importance rankings (Figure 5). Figure 5A-D show that the R^2 values of the model results exceeded 0.6, indicating a high model fit and a strong correlation between WER, SER, and the selected climate variables.

The results of the RF model (Figure 5) showed significant differences in the main climate-controlling factors between WER and SER on the interannual scale. Before 1991, the main climate-controlling factor influencing changes in WER was the North Atlantic oscillation (NAO; explaining 10.43%; $p<0.01$), while after 1991, the dominant factor shifted to cloud fraction, which explained 11.84% ($p<0.01$). Over the past half-century, changes in WER in NWC have also

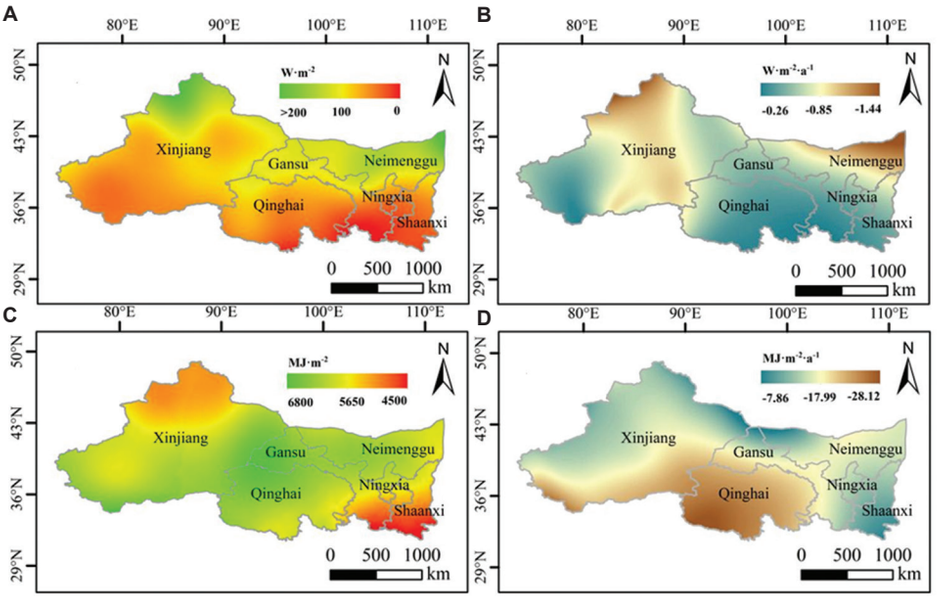

Figure 4. Spatial characteristics of wind and solar energy resources from 1961 to 2019. (A) Spatial distribution of wind energy resources; (B) Spatial trends of wind energy resources; (C) Spatial distribution of solar energy resources; (D) Spatial trends of solar energy resources.

Table 2. Correlation of climate factors with wind and solar energy resources before and after the abrupt change

Index	T	P	RH	CT	AO	ENSO	NAO	PDO	SOI
Wind									
Before	−0.306	−0.233	−0.324	0.208	−0.432	−0.019	−0.584*	−0.303	−0.156
After	−0.316	0.021	0.516*	−0.584*	−0.236	0.091	−0.221	0.273	−0.188
Solar									
Before	−0.464	−0.243	−0.553*	0.121	−0.282	0.013	−0.193	−0.224	0.044
After	0.518*	0.393	0.424	0.261	0.359	0.455	0.589*	0.746**	−0.612*

Notes: *p<0.05; **p<0.01.
Abbreviations: AO: Arctic oscillation; CT: Cloud fraction; ENSO: El Niño-southern oscillation; NAO: North Atlantic oscillation; P: Precipitation; PDO: Pacific decadal oscillation; RH: Relative humidity; SOI: Southern oscillation; T: Temperature.

been significantly affected by relative humidity and temperature (p<0.05). This indicates that after 1991, the climate-driving mechanism of WER shifted from being primarily controlled by air-sea circulation to being more influenced by inter-regional climate variability. In contrast, for SER, the main climate-controlling factors changed before and after 2005. Before 2005, temperature, relative humidity, and arctic oscillation (AO) were the dominant influences (explaining 31.34%). After 2005, the primary factors shifted to the Pacific decadal oscillation (PDO), NAO, and Southern oscillation, with an explanatory power of 29.59%. This shift suggests that SER transitioned from being influenced mainly by regional climate conditions to being increasingly affected by teleconnections associated with ASC. Overall, both WER and SER have been significantly influenced by temperature and relative humidity throughout most of the past half-century, indicating that global warming is closely associated with the observed decline in WER and SER in NWC. Previous studies have shown that global warming has exacerbated the warming and wetting trends in NWC to some extent.[10-13] Furthermore, changes in temperature and relative humidity can significantly alter the pressure gradient force and cloud cover in the region, and variations in cloud cover directly affect solar radiation. In addition, after 2005, the dominant climate-controlling factor for SER was ASC, indicating that the air-sea cycle between

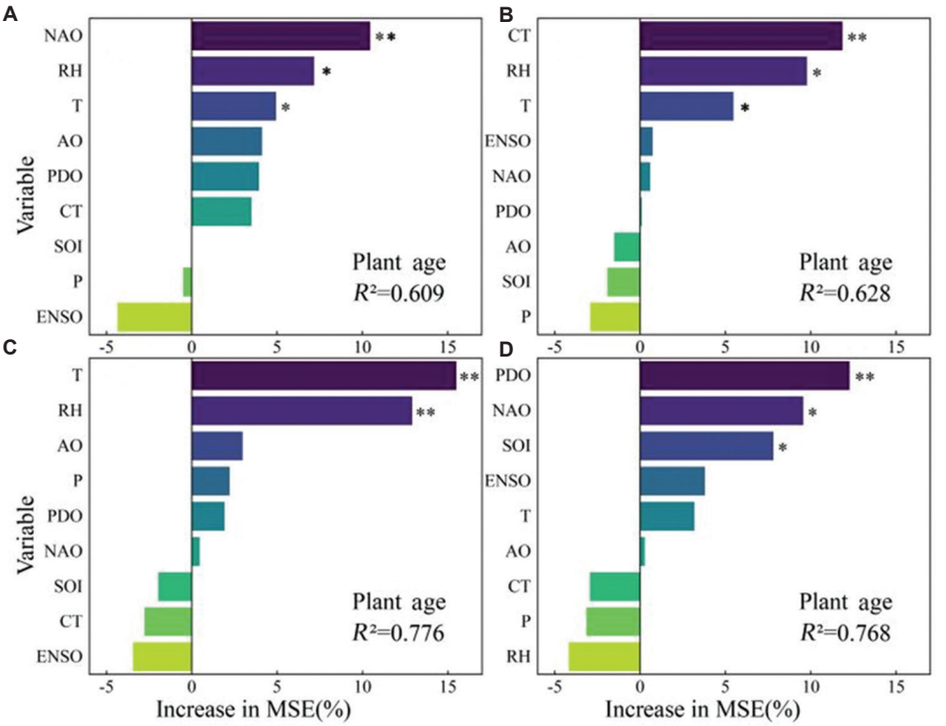

Figure 5. Interpretation ratio of wind energy resources (WER) and solar energy resources (SER) before and after abrupt change by climatic factors. (A) Interpretation ratio of climate factors for WER before the abrupt change; (B) Interpretation ratio of climate factors for WER after the abrupt change; (C) Interpretation ratio of climate factors for SER before the abrupt change; (D) Interpretation ratio of climate factors for SER after the abrupt change.

Notes: *p<0.05, **p<0.01.

Abbreviations: AO: Arctic oscillation; CT: Cloud fraction; ENSO: El Niño-southern oscillation; NAO: North Atlantic oscillation; P: Precipitation; PDO: Pacific decadal oscillation; RH: Relative humidity; SOI: Southern oscillation; T: Temperature.

land and ocean gradually became the primary driver of inter-regional microclimate changes. Therefore, greater attention should be given to global-scale climate models in future predictions and assessments of WER and SER.

4. Discussion

4.1. Sea-air circulation mechanism of wind and SER

NWC, as an important part of the arid region of Central Asia, has low urbanization levels and sparse vegetation cover. Over the past half-century, regional climate change has been the main driver of changes in WER and SER in NWC.[12,13] Because China is located in the eastern part of Eurasia and adjacent to the Pacific Ocean, its land surface gains and loses heat more rapidly than the ocean due to the ocean's higher specific heat capacity.[22-24] Meanwhile, existing studies have shown that global warming has significantly intensified the East Asian summer monsoon and other monsoon circulations.[25-28] On one hand, compared to the ocean, climate warming has a more pronounced effect on the land surface, resulting in a larger sea–land thermal contrast, which further enhances summer monsoon circulation. On the other hand, the variability of the AO index is influenced by winter temperatures in the mid-to-high latitudes of the Northern Hemisphere. In years when the AO index was strong, the intensity of the East Asian westerly jet, the north wind in mid-to-high latitudes, and the East Asian winter monsoon all exhibited a weakening trend (Figure 6), thereby reducing surface wind speeds across China during the same period. This also affects solar radiation by altering cloud cover, atmospheric water vapor, and haze levels in China.[29,30]

Recent studies have shown that since the 1990s, global cloud cover has decreased significantly. This reduction in cloud cover has contributed to a notable increase in global surface solar radiation.[31] As increased solar radiation directly heats the entire

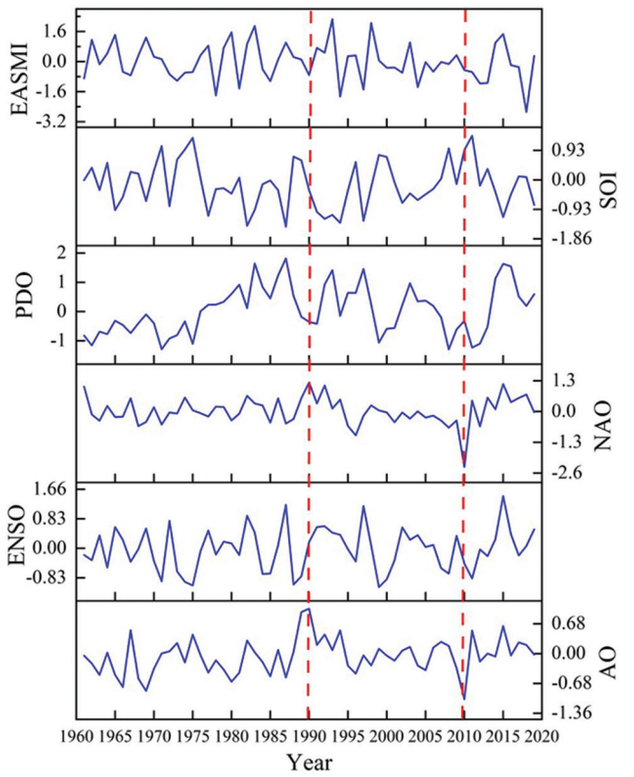

Figure 6. Interannual variation of air–sea circulation indices from 1961 to 2019

Note: Data are derived from the United States National Oceanic and Atmospheric Administration (http://www.esrl.noaa.gov/psd/enso/).

Abbreviations: AO: Arctic oscillation; EASMI: East Asian summer monsoon; ENSO: El Niño-southern oscillation; NAO: North Atlantic oscillation; PDO: Pacific decadal oscillation; SOI: Southern oscillation.

atmosphere, it reduces the thermal contrast between the upper atmosphere and the ground, diminishing the positive effects of ASC, and thereby significantly reducing WER. The RF model results further support this – before 1991, NAO was the dominant climatic factor influencing WER; after 1991, cloud fraction became the main controlling factor. Compared to SER, although the global surface solar radiation has generally increased, this rise has been concentrated mainly in the Southern Hemisphere and Europe. In contrast, SER in NWC has shown a significant declining trend since the 1990s. This is partly due to the more rapid increase in daily maximum temperatures before 2000 compared to after 1990, along with a marked greening trend in the northwest region after 2000.[31] Increased atmospheric water vapor and vegetation cover also led to significant reductions in surface solar radiation. Consequently, after 2006, SER in the NWC shifted from being primarily influenced by temperature to being controlled by ASC.

In addition, the PDO index fluctuated synchronously with the Aleutian low and Mongolian high in winter. The zonal sea–land pressure difference also changed with the PDO index, which altered the strength of the East Asian winter monsoon, resulting in the weakening of surface wind speeds and changes in solar radiation.[32,33] Moreover, the El Niño-southern oscillation index is the strongest circulation signal in air–sea interactions and is a major forcing factor in the interannual variability of the East Asian monsoon.[33,34] Although the NAO index can influence the intensity of the East Asian monsoon by modulating the AO index, its impact is relatively limited.[33,34] Previous studies have also indicated that Arctic warming, sea ice melting, and aerosol changes affect the meridional pressure gradient, thermal gradient, and low-level circulation in the Northern Hemisphere. These factors contribute to the weakening of the mid-latitude westerly jet and the strengthening of meridional circulation. Meanwhile, surface cooling caused by aerosols reduces the sea–land temperature difference. The combined effect of these phenomena leads to significant changes in monsoon circulation and regional climate. However, these effects may be masked by the natural weakening phase of certain circulation systems, thereby reducing their apparent contribution.

4.2. Future development and management of wind and SER

As typical climate-dependent resources, WER and SER exhibit significant seasonal and regional variations in their development and utilization and are strongly constrained by climate change.[35,36] According to the intergovernmental panel on climate change report, the frequency of regional extreme climate events has increased in recent years due to global warming.[37] As an arid and semi-arid region, NWC has a low threshold for ecosystem resilience and system stability, making it more vulnerable to extreme events such as heavy precipitation, persistent high temperatures, and severe dust storms.[37,38] Under future climate change scenarios, the increasing frequency of extreme climate events is likely to pose considerable challenges to the development, supply, and demand of WER and SER. Furthermore, the large-scale deployment of WER and SER inevitably requires substantial land use. Infrastructure such as rotating turbine blades and photovoltaic arrays can have observable impacts on local ecosystems, including reduced vegetation growth near installations and habitat loss for wildlife. However,

comprehensive life-cycle assessments indicate that the climate mitigation potential and socioeconomic benefits derived from the development of WER or SER far outweigh their localized environmental costs under present technological frameworks.[8,13] In the context of urgent decarbonization efforts, scaling up renewable energy infrastructure remains the most feasible strategy for achieving net environmental benefits at the ecosystem scale.

Therefore, in the future stages of development, utilization, and operational management of WER and SER in NWC, regional government needs to improve their capacity for climate monitoring and forecasting.[39,40] This includes analyzing climate and weather changes across multiple timescales, enhancing regional resource development and utilization plans, and advancing the intelligence and adaptability of the regional power grid. To address the instability of wind and solar power generation caused by climatic and geographical variability, this instability can be mitigated by expanding the spatial scale or temporal scale of operations through regional coordination.[41-43] Based on the spatial and temporal characteristics of WER and SER in the region, the proportion of wind and photovoltaic power generation should be adjusted accordingly. A coupled WER–SER collaborative power generation model, supported by hydropower,[8,13] should be developed to reduce the curtailment of wind and photovoltaic power in the region and to improve the overall utilization efficiency of the new energy power system. Accurate forecasting of future regional wind and solar power generation is critical for power system scheduling, load balancing, and generation planning.[44-46]

4.3. Limitations of the study

This study elucidated the interannual dynamics of changes in WER and SER in the NWC and quantified the driving processes behind these changes. Although the findings provide data support and a theoretical basis for the development of WER and SER in the region, the development, and utilization of these resources involve variations on daily and even hourly timescales. The present use of daily and monthly datasets may not fully capture the key signals of WER and SER variability. Therefore, the availability of high-resolution spatiotemporal datasets will be essential to support the effective development and utilization of WER and SER in the future. In subsequent research, more in-depth studies should be conducted at shorter timescales, along with evaluations that incorporate existing development technologies and methods for WER and SER.

5. Conclusion

Across the synergistic application of meteorological station networks, reanalysis datasets, and machine learning models, the following key findings were obtained:

(i) The results of the trend and wavelet analysis indicate that WER and SER demonstrated regime shifts characterized by distinct phases – initial growth, transitional decline, and accelerated depletion – superimposed with significant 29 – 30-year oscillation signals.

(ii) Spatial evolution patterns revealed clear differences between WER and SER. WER showed an increasing trend from south to north, while SER displayed a decreasing trend from the central region to the surrounding areas.

(iii) The RF model results demonstrated that the main controlling factors for WER shift from air–sea circulation dominance to inter-regional climate variations, while those for SER exhibited the opposite trend. This was mainly attributed to a significant reduction in cloud cover and a notable slowdown in the rate of increase of daily maximum temperatures.

(iv) This study establishes that synoptic-scale circulation reorganizations outweigh local anthropogenic impacts in determining the viability of renewable energy. Moreover, the development and utilization of WER and SER will increasingly depend on high-resolution spatiotemporal datasets in future planning and assessments.

Acknowledgments

None.

Funding

This work was jointly supported by the Guangdong University of Petrochemical Technology (GDUPT) Talents Recruitment Project (grant number: 2019rc098), the Academic Affairs of GDUPT for the Goal Problem-Oriented Teaching Innovation and Practice Project (grant number: 41967038), and the Scientific Research Innovation Foundation of Yunnan Province (grant number: KC-242410028).

Conflict of interest

The authors declare that they have no known competing financial interests or personal relationships that could

have appeared to influence the work reported in this paper.

Author contributions

Conceptualization: Shuyue Qin, Bingyue Wen, Taohui Li
Data curation: Shuyue Qin, Bingyue Wen
Formal analysis: Shuyue Qin, Bingyue Wen, Ruei-Yuan Wang, Hongbei Guo
Investigation: Ruei-Yuan Wang, Dongping Yu, Yanfang Jin
Methodology: Shuyue Qin, Bingyue Wen, Taohui Li
Resources: Ruei-Yuan Wang, Taohui Li
Software: Shuyue Qin, Bingyue Wen, Yunxia Ma
Validation: Wei Bao, Xuexian Wang, Zihan Yang, Yunxia Ma
Writing – original draft: Shuyue Qin, Bingyue Wen, Taohui Li
Writing – review & editing: Shuyue Qin, Bingyue Wen, Taohui Li

Availability of data

Data are available from the corresponding author Taohui Li (taohui0813@foxmail.com) upon request.

References

1. Randerson JT, Liu H, Flanner MG, *et al*. The impact of boreal forest fire on climate warming. *Science*. 2006;314(5802):1130-1132. doi: 10.1126/science.1132075
2. Palutikof JP, Boulter SL, Field CB, *et al*. Enhancing the review process in global environmental assessments: The case of the IPCC. *Environ Sci Policy*. 2023;139:118-129. doi: 10.1016/J.ENVSCI.2022.10.012
3. Terlouw T, Savvakis N, Bauer C, McKenna R, Arampatzis G. Designing multi-energy systems in mediterranean regions towards energy autonomy. *Appl Energy.* 2025;377(PB):124458. doi: 10.1016/J.APENERGY.2024.124458
4. Arnaoutakis GE, Georgia K, Eirini D, Katsaprakakis A. Combined operation of wind-pumped hydro storage plant with a concentrating solar power plant for insular systems: A case study for the island of rhodes. *Energies*. 2022;15(18):6822. doi: 10.3390/EN15186822
5. Papaefthymiou G, Dragoon K. Towards 100% renewable energy systems: Uncapping power system flexibility. *Energy Policy*. 2016;92:69-82. doi: 10.1016/j.enpol.2016.01.025
6. Kim SK, Park S. Impacts of renewable energy on climate vulnerability: A global perspective for energy transition in a climate adaptation framework. *Sci Total Environ*. 2023;859(P1):160175. doi: 10.1016/J.SCITOTENV.2022.160175
7. Arnaoutakis GE, Papadakis N, Katsaprakakis KD. CombiCSP: A python routine for dynamic modeling of concentrating solar power plants. *Softw Impacts*. 2022;13:100367. doi: 10.1016/J.SIMPA.2022.100367
8. Lv A, Li T, Zhang W, Liu Y. Spatiotemporal distribution and complementarity of wind and solar energy in China. *Energies*. 2022;15(19):7365. doi: 10.3390/EN15197365
9. Feng Y, Que L, Feng J. Spatiotemporal characteristics of wind energy resources from 1960 to 2016 over China. *Atmos Oceanic Sci Lett*. 2020;13(2):136-145. doi: 10.1080/16742834.2019.1705753
10. Liepert BG. Observed reductions of surface solar radiation at sites in the United States and world from 1961 to 1990. *Geophys Res Lett*. 2002;29(10):61-64. doi: 10.1029/2002GL014910
11. Wild M, Ohmura A, Makowski K. Impact of global dimming and brightening on global warming. *Geophys Res Lett*. 2007;34(4):1-4. doi: 10.1029/2006GL028031
12. Li T, Lv A, Zhang W, Liu Y. Spatiotemporal characteristics of watershed warming and wetting: The response to atmospheric circulation in arid areas of northwest China. *Atmosphere*. 2023;14(1):151. doi: 10.3390/ATMOS14010151
13. Li T, Liu Y, Lv A. Review of research on the present situation of development and resource potential of wind and solar energy in China. *Energies*. 2024;17(16):4158. doi: 10.3390/EN17164158
14. Jakub J, Mohammed G, Pietro CE, *et al*. Complementarity of wind and solar power in North Africa: Potential for alleviating energy droughts and impacts of the North Atlantic Oscillation. *Renew Sustain Energy Rev*. 2024;191:114181. doi: 10.1016/J.RSER.2023.114181
15. Sawadogo W, Reboita SM, Faye A, *et al*. Current and future potential of solar and wind energy over Africa using the regCM4 CORDEX-CORE ensemble. *Clim Dyn*. 2020;57(10):1647-1672. doi: 10.1007/s00382-020-05377-1
16. Bin H, Aifeng L, Jianjun W, Lin Z, Ming L. Drought hazard assessment and spatial characteristics analysis in China. *J Geogr Sci*. 2011;21(02):235-249. doi: 10.1007/s11442-011-0841-x
17. Fan L, Lv A, Zhang W. Temporal-spatial variation characteristics of drought and its relationshipwith atmospheric circulation in Qinghai province. *J Arid Land Res Environ*. 2021;35(12):60-65. doi: 10.13448/j.cnki.jalre.2021.326
18. Zhu R, Wang Y, Xiang Y, *et al*. Study on climate

characteristics and development potential of wind energy resources in China. *Acta Energiae Solaris Sinica*. 2021;42(6):409-418.
doi: 10.19912/j.0254-0096.tynxb.2020-0130

19. Zhang S, Li X. Study on application of ERA5 data to solar energy resource assessment over China's region. *Acta Energiae Solaris Sinica*. 2023;44(05):280-285.
doi: 10.19912/j.0254-0096.tynxb.2021-1604
20. Yin J, Hu W, Chen A, Li T, Zhang W. Human-caused increases in organic carbon burial in plateau lakes: The response to warming effect. *Sci Total Environ*. 2024;937:173556.
doi: 10.1016/J.SCITOTENV.2024.173556
21. Li T, Zhang W, Lv A, Liu Y. Temporal and spatial characteristics of heat resources in growing season in yunnan province, China. *Mt Res*. 2023;41(3):361-374.
doi: 10.16089/j.cnki.1008-2786.000754
22. Chen J, Xu D, Luo Y, Zheng X, Zhou C, Kang W. Changes in solar radiation and their climatic influences over yunnan-guizhou plateau for 1961 ~ 2019. *Res Environ Yangtze Basin*. 2012;21(S1):179-184.
23. Liu X, Jiang Y, Ren G, Liang X, Zhang C. Effect of urbanization and observation environment change on wind speed trend in hebei province, China. *Plateau Meteorol*. 2009;28(2):433-439.
24. Lu Q, Rao J, Liang Z, *et al*. The sudden stratospheric warming in January 2021. *Environ Res Lett*. 2021;16(8):084029.
doi: 10.1088/1748-9326/AC12F4
25. Hongming Y, Yuan Y, Guirong T, Yucheng Z. Possible impact of sudden stratospheric warming on the intraseasonal reversal of the temperature over East Asia in winter 2020/21. *Atmos Res*. 2022;268:106016.
doi: 10.1016/J.ATMOSRES.2022.106016
26. Wang P, Yang J, Zhang Q, He J, Wang D, Lu D. Climate change characteristic of northwest China in recent half century. *Adv Earth Sci*. 2007;6:649-656.
27. Lan L, Li D. Interannual and interdecadal anomaly features of siberian high andtheir impact on winter temperature of China. *Plateau Meteorol*. 2016;35(3):662-674.
doi: 10.7522/j.issn.1000-0534.2016.00022
28. Sun X, Wang P, Zhi H, Guo D. Analysis and comparison of several mongolian high circulation indicesand their relationship with temperature anomaly of China in winter. *Plateau Meteorol*. 2010;29(6):1493-1500.
29. Sun G, Li Y, Li S. The differences in cloud vertical structures between active and break spells of the East Asian summer monsoon based on cloud sat data. *Atmos Res*. 2019;224:157-167.
doi: 10.1016/j.atmosres.2019.03.035
30. Sun G, Li Y, Lu J. Why is there a tilted cloud vertical structure associated with the Northward advance of the East Asian summer monsoon. *Atmos Res*. 2019;215:317-325.
doi: 10.1016/j.atmosres.2018.09.013
31. Zhong Z, He B, Chen HW, *et al*. Reversed asymmetric warming of sub-diurnal temperature over land during recent decades. *Nat Commun*. 2023;14(1):7189.
doi: 10.1038/S41467-023-43007-6
32. Zheng F, Yuan Y, Ding Y, *et al*. The 2020/21 extremely cold winter in China influenced by the synergistic effect of la niña and warm arctic. *Adv Atmos Sci*. 2021;39(4):546-552.
doi: 10.1007/S00376-021-1033-Y
33. Liu Y, Wu C, Jia R, Huang J. An overview of the influence of atmospheric circulation on the climate inarid and semi-arid region of Central and East Asia. *Sci China Earth Sci*. 2018;48(9):1141-1152.
doi: 10.1007/s11430-017-9202-1
34. Liu Y, Huang J, Shi G, *et al*. Aerosol optical properties and radiative effect determined from sky-radiometer over Loess Plateau of Northwest China. *Atmos Chem Physics*. 2011;11(252):11455-11463.
doi: 10.5194/acp-11-11455-2011
35. Fang W, Yang C, Liu D, *et al*. Assessment of wind and solar power potential and their temporal complementarity in China's northwestern provinces: Insights from ERA5 reanalysis. *Energies*. 2023;16(20):7109.
doi: 10.3390/en16207109
36. Lu H, Wang C, Li Q, Wiser R, Porter K. Reducing wind power curtailment in China: Comparing the roles of coal power flexibility and improved dispatch. *Clim Policy*. 2019;19(5):623-635.
doi: 10.1080/14693062.2018.1546164
37. Sun J, Wang Y, Yang X, Lu Z, He Y, Chao Q. Analysis of spatial and temporal variation character of climate risks of wind and solar. *Electric Power*. 2023;56(5):1-10.
doi: 10.11930/j.issn.1004-9649.202211009
38. Wu J, Yan Y. Projection and outlook of future wind energy and solar energy resources in China. *Energy China*. 2023;45(Z1):49-58.
doi: 10.3969/j.issn.1003-2355.2023.01.008
39. Xue-Jie G, Mei-Li W, Giorgi F. Climate change over china in the 21st century as simulated by Bcc_CSM1.1-RegCM4.0. *Atmos Oceanic Sci Lett*. 2013;6(5):381-386.
40. Li D, Feng J, Dosio A, Qi J, Xu Z, Yin B. Historical evaluation and future projections of 100-m wind energy potentials over CORDEX-East Asia. *J Geophys Res Atmos*. 2020;125(15):e2020JD032874.
doi: 10.1029/2020JD032874
41. Jurasz J, Mikulik J, Dabek PB, Guezgouz M, Kaźmierczak B. Complementarity and 'resource droughts' of solar and wind energy in Poland: An ERA5-based analysis. *Energies*. 2021;14(4):1118.
doi: 10.3390/EN14041118
42. Puspitarini HD, François B, Zaramella M, Brown C, Borga M. The impact of glacier shrinkage on energy production from hydropower-solar complementarity in alpine river basins. *Sci Total Environ*. 2020;719:137488.

doi: 10.1016/j.scitotenv.2020.137488
43. Han S, Zhang L, Liu Y, *et al*. Quantitative evaluation method for the complementarity of wind-solar-hydro power and optimization of wind-solar ratio. *Appl Energy.* 2019;236:973-984.
doi: 10.1016/j.apenergy.2018.12.059
44. Guan X. *Development and Utilization of Wind and Solar Energy*. Beijing: China Meteorological Press; 2018. p. 84-200.
45. Liu L, Wang Y, Wang Z, *et al*. Potential contributions of wind and solar power to China's carbon neutrality. *Res Conserv Recycl*. 2022;180:106158.
doi: 10.1016/J.RESCONREC.2022.106155
46. Ekanayake P, Peiris AT, Jeevani JM, Jayasinghe W, Rathnayake U. Development of wind power prediction models for pawan danavi wind farm in Sri Lanka. *Math Probl Eng*. 2021;2021:893713.
doi: 10.1155/2021/4893713